THE AMERICAN SOCIETY OF MECHANICAL ENGINEERS
345 E. 47th St., New York, N.Y. 10017

97-GT-95

Experimental Study of the Unsteady Aerodynamics in a Linear Cascade with Low Reynolds Number Low Pressure Turbine Blades

Christopher G. Murawski
Rolf Sondergaard and Richard B. Rivir
Aeropropulsion and Power Directorate,
Wright Laboratory, USAF
Wright Patterson AFB, OH.

Kambiz Vafai
Department of Mechanical Engineering
Ohio State University, Columbus, OH.

Terrence W. Simon
Department of Mechanical Engineering
University of Minnesota, Minneapolis, MN.

Ralph J. Volino
Department of Mechanical Engineering
U.S. Naval Academy, Annapolis, MD.

ABSTRACT

Low pressure turbines in aircraft experience large changes in flow Reynolds number as the gas turbine engine operates from take-off to high altitude cruise. Low pressure turbine blades are also subject to regions of strong acceleration and diffusion. These changes in Reynolds number, strong acceleration, as well as elevated levels of turbulence can result in unsteady separation and transition zones on the surface of the blade.

An experimental study was conducted in a two-dimensional linear cascade, focusing on the suction surface of a low pressure turbine blade. The intent was to assess the effects of changes in Reynolds number, and freestream turbulence intensity. Flow Reynolds numbers, based on exit velocity and suction surface length, have been varied from 50,000 to 300,000. The freestream turbulence intensity was varied from 1.1 to 8.1 percent.

Separation was observed at all test Reynolds numbers. Increasing the flow Reynolds number, without changing freestream turbulence, resulted in a slightly rearward movement of the onset of separation and shrinkage of the separation zone.

Increasing the freestream turbulence intensity, without changing Reynolds number resulted in a shrinkage of the separation region on the suction surface.

Increasing both flow Reynolds numbers and freestream turbulence intensity compounded these effects such that at a Reynolds number of 300,000 and a freestream turbulence intensity of 8.1%, the separation zone was almost nonexistent.

The influences on the blade's wake from altering freestream turbulence and Reynolds number are also documented. The width of the wake and velocity defect rise with a decrease in either turbulence level or chord Reynolds number.

Numerical simulations were performed in support of experimental results. The numerical results compare well qualitatively with the low freestream turbulence experimental cases.

NOMENCLATURE

Cp = Local pressure coefficient
P_{Si} = Static pressure along the blade surface
$P_{T_{in}}$ = Total pressure at inlet to blade set
$\overline{P_{T_{out}}}$ = Average total pressure behind the blade row
$P_{T_{out,i}}$ = Local total pressure behind the blade row
Re = Reynolds number (U_{OUT} (SSL) / υ)
SSL = Suction surface length
Tu = Freestream turbulence intensity ($u'_{rms} / \bar{u}_{local}$)
U_{OUT} = Average velocity out of the blade set
u'_{rms} = Root mean square of the fluctuating component of streamwise velocity
$\bar{u}_{local}$ = Local mean streamwise velocity
γ = Loss coefficient
υ = Kinematic viscosity
ρ = Density

BACKGROUND

As a result of reduced pressures while maintaining relatively high temperatures, the low pressure turbine experiences large changes in chord Reynolds number as the gas turbine engine operates from take-off to cruise conditions. As Reynolds number drops, flow separation zones expand and regions of transitional flow lengthen. The end result is a degradation in performance. Sharma, et al. (1994) documented this trend.

Mayle (1991), in a review of the role of laminar to turbulent transition in gas turbine engines, concluded that it has a major impact

Presented at the International Gas Turbine & Aeroengine Congress & Exhibition
Orlando, Florida — June 2–June 5, 1997

on blade performance. He defined three modes of transition; natural transition, bypass transition and separated-flow transition. Natural transition is defined by the classical development and break-up of Tollmien-Schlichting waves. Bypass transition bypasses the formation of Tollmien-Shlichting linear instability waves, going to turbulent spots directly. The spots merge to yield a turbulent boundary layer. Separated-flow transition occurs when a boundary layer separates, and transition proceeds in the free-shear-layer flow above the separation bubble. The transition region propagates toward the wall giving a growing turbulent zone until the flow reattaches as a fully turbulent boundary layer. Because of the elevated levels of freestream turbulence, curvature, and the diffusion in the boundary layer, the transition processes most likely to occur on a turbine blade are bypass and separated-flow transition.

Several recent papers relevant to the present study are:

Rivir (1996) presented an experimental and computational effort which investigated the effect of turbulence intensity and turbulence length scale on the transition zone in a low pressure turbine cascade. He concluded that changes in turbulence intensity and turbulence length scale did not affect the location of transition onset. However they do affect the length of transition.

Halstead et al. (1995) reported the results of an extensive experimental study of compressor and low pressure turbine flows. While their experiment concentrated on turbine flow that contained wake disturbances, they concluded that the performance of highly loaded, low pressure turbine blades are dependent on flow transition and separation behavior. Computational results could not adequately predict transition regions.

Baughn et al. (1995) reported experimental results which concentrated on transition and separation on turbine blades at low Reynolds numbers with freestream turbulence intensities of 1%, and 10%. They documented the movement forward of the transition point as freestream turbulence intensity was increased. Rivir, et al. (1996) conducted a computational study of the same geometry at various Reynolds numbers but without turbulence. Their results show that a low pressure turbine blade separates as Reynolds number decreases below 100,000.

In the present paper, we focus on Reynolds number and turbulence level effects on a low pressure turbine airfoil and document the effect of these influences on the airfoil wake.

EXPERIMENTAL METHOD

Experimental Apparatus

A linear, 2-D airfoil cascade at the Air Force Institute of Technology at Wright Patterson Air Force Base, was employed to study a low pressure turbine airfoil. A schematic of the test apparatus is provided in Fig. 1. Air is pulled through the apparatus by a 20 HP motor operating a Buffalo Forge centrifugal blower in the suction mode. Air flow through the test rig is controlled by an Allen-Bradley 1336 variable speed motor controller.

The wind tunnel inlet bell-mouth directs the flow through a 53 cm square by 20 cm deep honeycomb flow straightener. The flow continues through a 7:1 converging nozzle to the 11.4 cm by 40.6 cm flow channel.

The inlet freestream turbulence intensity is elevated by a passive turbulence grid which is located 1.45 m upstream of the cascade row. The grid is a wooden square mesh of 13 mm square bars arranged with a 25.4 mm center-to-center spacing. The turbulence grid is removed to provide low levels of inlet freestream turbulence.

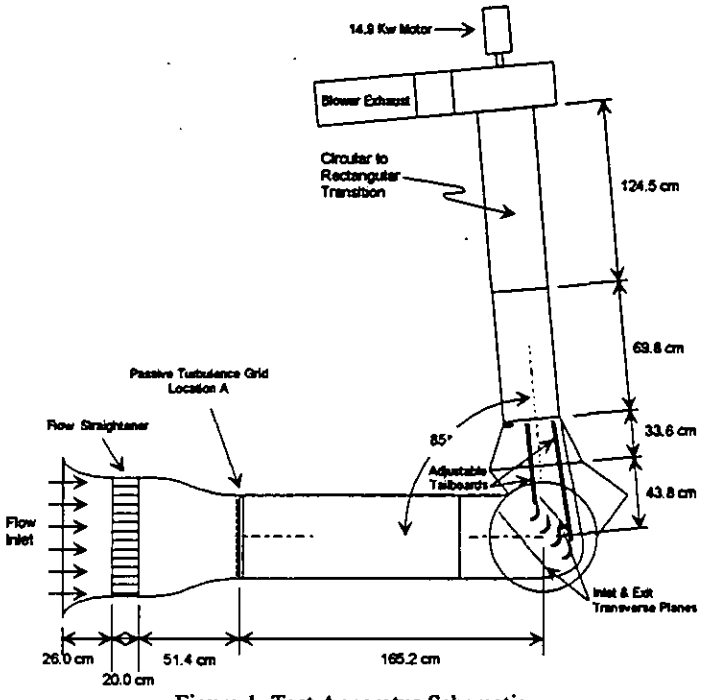

Figure 1. Test Apparatus Schematic

The cascade used in this experiment contains four geometrically identical, low pressure turbine blades with an axial chord length of 11.4 cm and a span-to-chord length aspect ratio of 1.0. The suction surface length is 15.24 cm. The pitch-to-chord ratio (solidity) is 0.8 and the flow is turned through 95°.

Instrumentation

Instantaneous local velocities are measured using a single element, hot-film probe (TSI model #:1210-10 or 1210-20). Boundary layer profiles were recorded by traversing the single element, hot-film probe, in-line with the flow, across the boundary layer. Velocities in the wake were also recorded using a single element, hot-film probe. Mean velocity and total pressure measurements were with a United Sensor pitot-static probe, model number PDA-8-F-6-K1.

The airfoil surface static pressures are measured using 22 static pressure ports installed at midspan on the surface of one blade. The ports are connected to stainless steel tubing which manifolds to a Scanivalve selector (Model # 48J9-1). Three Validyne pressure transducers were used (Model #: DP45-14, DP45-20, DP45-22) to cover the range of cascade pressures. Voltages were acquired by a Hewlett-Packard 3852 Data Acquisition Unit controlled by a 486 personal computer. National Instruments LabVIEW software was utilized for data acquisition.

The experimental uncertainties were established based on knowledge and experience of the instrumentation, and calculations of the propagation of uncertainty by using the method of Kline and

McClintock (1953). The uncertainty of the velocity measurements resulting from pressure transducers and the single wire, hot-film probe was estimated to be less than 2%. The maximum uncertainty in the pressure coefficient and loss coefficient are estimated to be less than 4%.

Computational Method

Numerical simulations of the experimental rig were performed using VBI2D, an unsteady, two-dimensional, Navier-Stokes code developed by the Allison Engine Company under contract to the United States Air Force (Rao et al. (1994)). The computational grid used in this study is illustrated in Fig. 2. The grid is an overlaid (Chimera) combination of a rectangular H grid (67X59) and a body fitted hyperbolic O grid (101X41). The rectangular grids are used to resolve the free stream flow and the O grids are used to resolve the regions of high shear associated with the boundary layer. The steady solution of the code is based on a five-step, Runge Kutta relaxation method that incorporates residual smoothing to accelerate convergence to the final solution. The code implements a Baldwin-Lomax (1978), two-layer, algebraic turbulence model and the Baldwin-Lomax point transition model which assumes that transition occurs when the calculated C_μ = 14. Resolution of the inner boundary layer was a significant driver for selection of the O grid spacing, with the first grid point at a y+ ≤ 1. Steady state residuals for converged calculations are of the order of 10e-6.

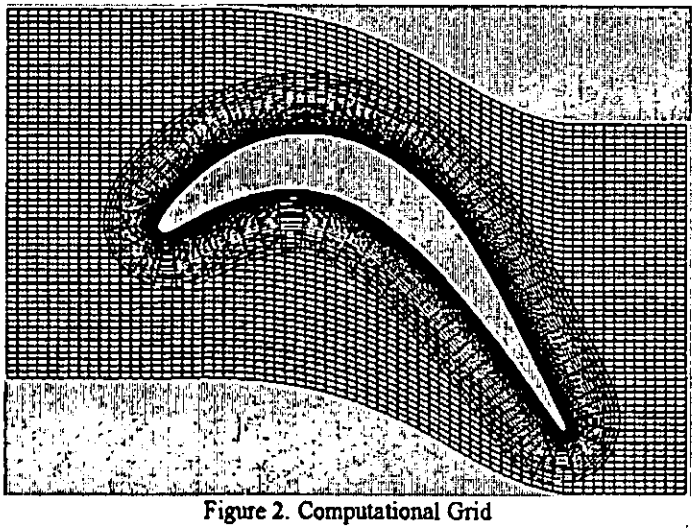

Figure 2. Computational Grid

RESULTS

Inlet Profile

To verify an acceptable inlet, a flow survey was performed using a single hot-film probe. The survey (Fig. 3) was taken one blade chord upstream of the leading edges at mid-tunnel height. Without a turbulence generation grid, the inlet flow turbulence intensity is uniform at 1.1%. The passive turbulence grid creates an inlet freestream turbulence level of 8.1%. Figure 3 shows the inlet axial flow velocity is uniform with and without the grid varying about the mean by less than 7.5%.

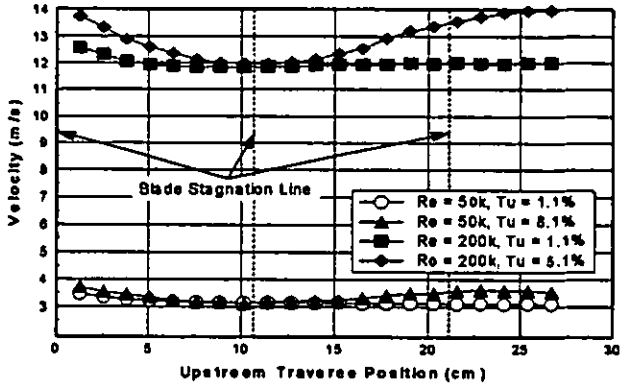

Figure 3. Inlet Velocity Survey

Loss Coefficient

Overall performance is documented with the loss coefficient.

$$\gamma = \frac{\left(P_{T_{in}} - \overline{P_{T_{out}}}\right)}{\frac{1}{2}\rho U_{OUT}^2} \qquad (1)$$

The inlet total pressure is measured one axial blade chord upstream. The outlet total pressure is the average of a traverse perpendicular to exit flow, and 2.54 cm behind a test blade. Figure 4 shows experimental and calculated loss coefficients. Computational results contain no freestream turbulence. The results show that blade losses increase as Reynolds numbers decrease. At Reynolds numbers below 100,000, the computational results contain a separated boundary layer that does not reattach. For Reynolds numbers greater than 100,000, the computational results contain a boundary layer that transitions to turbulence and remains attached. The transition in the calculated results occurs instantaneously. The separation and transition zones of the experimental results are affected by Reynolds number and freestream turbulence levels.

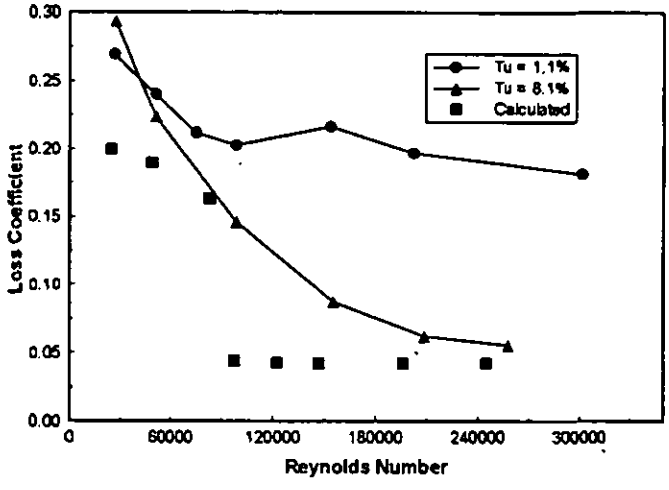

Figure 4. Loss Coefficient

The calculated and low freestream turbulence experimental results show that the loss coefficient increases sharply when Reynolds number is less than 100,000. The increase in loss coefficient at lower Reynolds number is caused by strong separation without reattachment, resulting in significantly larger wakes. The loss coefficient with freestream turbulence of 8.1% decreases continuously as Reynolds numbers are increased At higher Reynolds numbers the boundary layer reattaches and the separation zone continues to shrink, resulting in smaller wakes.

Boundary Layer Survey

Figure 5 shows measured velocity profiles in the boundary layer along the suction surface of the low pressure airfoil with the flow Reynolds number of 53,000 and 160,000, and a freestream turbulence level of 1.1%. Figure 5 provides a comparison of the measured velocity profiles at several axial chord locations. The velocity profiles are presented as a ratio of the local velocity divided by the maximum velocity in the boundary layer at each survey location.

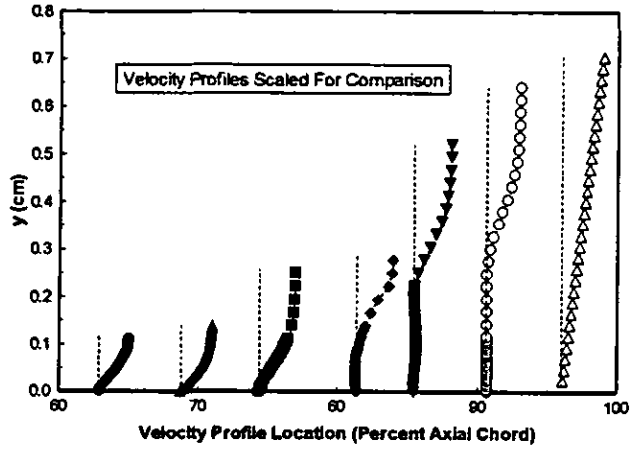

Figure 5a. Boundary Layer Velocity Survey, Re = 53k

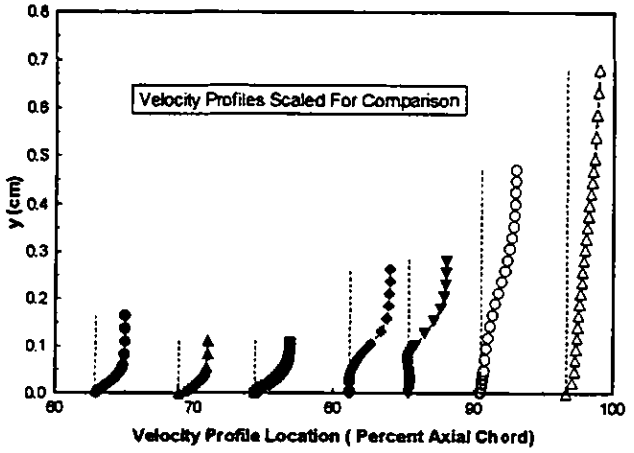

Figure 5b. Boundary Layer Velocity Survey, Re = 160k

Figure 5a illustrates that at a flow Reynolds number of 53,000, separation occurs on the suction surface before the traverse at 74% axial chord. Separation is observed when the velocity profile departs from the classic laminar flat plate boundary layer shape. At an axial chord of 90% the flow is still separated, and the boundary layer has grown in height to 0.457 cm. Figure 5b illustrates that with a flow Reynolds number of 160,000, flow separation has just begun at 74% of axial chord. The boundary layer does not grow as fast as in Fig. 5a, and the flow is about to reattach at 90% of axial chord.

Figure 6 shows local freestream turbulence intensity profiles at each measured velocity profile station. At a Reynolds number of 53,000, Fig. 6a confirms that the boundary layer has separated before 74% of axial chord as indicated by a near-wall region of uniform high level of turbulence. At 96% axial chord, the shape of the local freestream turbulence survey near the wall is similar to that of 90% axial chord, where the boundary layer is separated. This confirms that the boundary layer is still separated at 96% axial chord.

Figure 6b, similarly confirms the conclusions seen in the velocity boundary layer plot for Reynolds number of 160,000. In this case, flow separates at 74% of axial chord, which is later than the Reynolds number of 53,000 case. Increasing the Reynolds number results in a delay of the onset of separation, and the boundary layer reattaches.

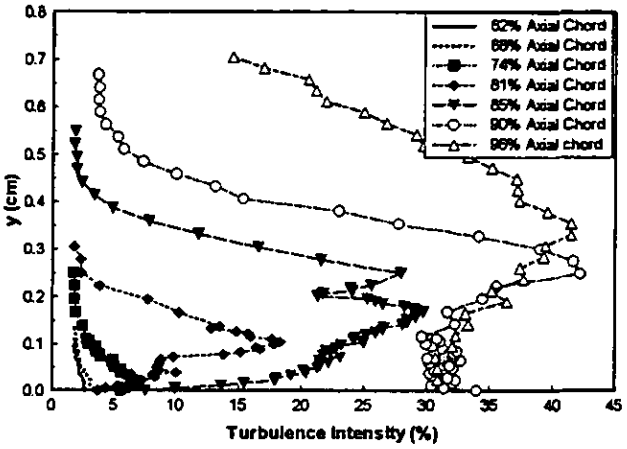

Figure 6a. Boundary Layer Turbulence Survey, Re = 53k

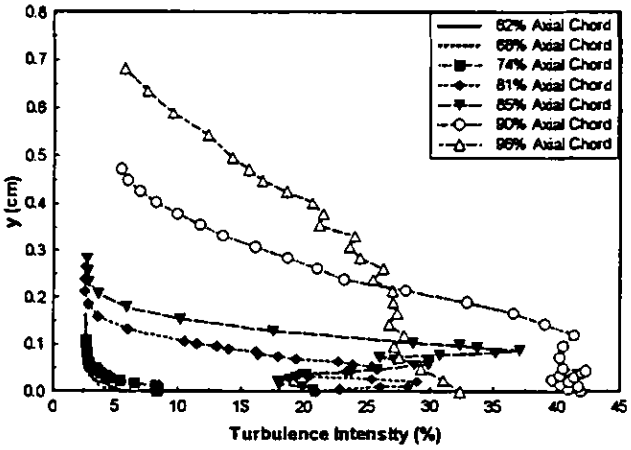

Figure 6b. Boundary Layer Turbulence Survey, Re = 160k

The rate at which the boundary layer grows, and its maximum thickness also is affected by Reynolds number and freestream

turbulence level. Lower Reynolds number cases have a larger separation zone on the suction side of the airfoil. In Fig. 4, the low Reynolds number cases have larger loss coefficients. In Fig. 5a, the lower Reynolds number case separates sooner, grows faster and does not reattach. These results are consistent with a larger pressure drop at the lower Reynolds number.

Surface Static Pressure Results

Surface static pressure surveys, presented in terms of pressure coefficients in Figs. 7 and 8, were conducted on the 2-D cascade test blade for a wide range of Reynolds numbers. Figure 7 presents the experimental and computational pressure coefficients for the suction surface of the turbine blade with freestream turbulence levels of 1.1% and 0%, respectively. Figure 8 contains experimental pressure coefficients for freestream turbulence levels of 8.1%.

Cp is the pressure coefficient defined by equation 2.

$$Cp = \frac{(PT_{in} - PS)}{\frac{1}{2}\rho U_{out}^2} \qquad (2)$$

Along the suction side surface, from 0 to 50 % of axial chord, the flow behaves similarly for all Reynolds numbers. The flow over the last 50% of the suction side surface is affected by changes in Reynolds number and freestream turbulence intensity.

Figure 7 includes curves illustrating the computational results for Re=50,000 and 200,000. When Re=200,000 the boundary layer remains attached and transitions to turbulent flow. For the case Re=50,000, separation occurs at 75% axial chord.

The measured velocity profiles for Tu=1.1% (Fig. 5), separate near 74% axial chord. The pressure coefficient profiles of Fig. 7 contain a terrace (flat zone) in this region. Gaster (1966) explained that the terrace is created by the initial portion of the separation bubble composed of a laminar shear layer and a dead air region. The shear layer then begins to interact with the separation bubble. A region of turbulent mixing occurs which may result in boundary layer reattachment. At the end of the dead air zone the magnitude of the velocity will increase near the wall. The initiation of transition appears as a region on the pressure coefficient curve that quickly falls off after the flat zone.

A terrace is present in the pressure coefficient profiles for all Reynolds numbers tested in Figs. 7 and 8. Separation occurs in the same region for all cases. Increasing the Reynolds number results in the beginning of transition moving forward. The exact location of separation, transition and reattachment cannot be determined until a more detailed study of the flow field is completed.

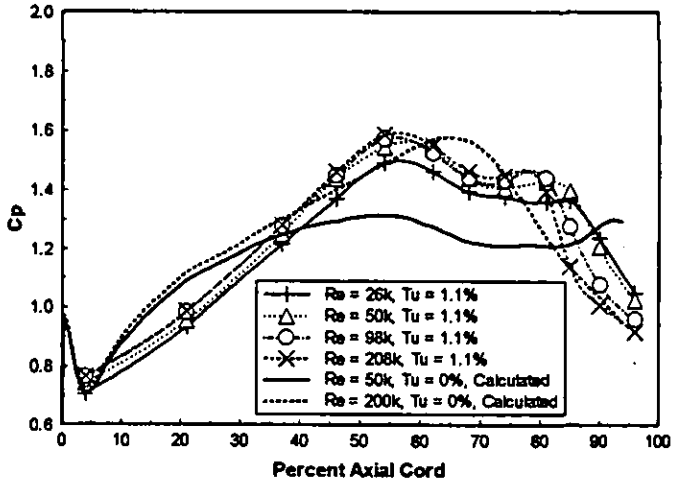

Figure 7. Surface Static Pressure Survey, Tu = 1.1%

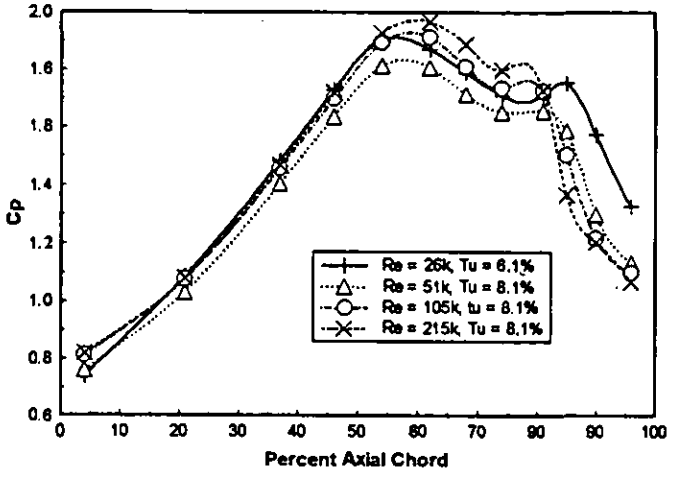

Figure 8. Surface Static Pressure Survey, Tu = 8.1%

Wakes

Changes in the size, length and location of the separation zones on the turbine blade influence the strength of the wake. Each point on Fig. 9 represents a local instantaneous velocity recorded while the hot film probe was being traversed parallel to and 2.54 cm behind the plane of the trailing edges of the 2-D cascade turbine blade. The size and shape of the wakes directly correlate with the loss coefficients in Fig. 4.

Figure 9a and 9b show wake surveys for a Reynolds number of 50,000, with and without the turbulence grid. The level of rms fluctuation is similar, however the width of the wake is diminished as the freestream turbulence increases. This results in a lower loss coefficient for the case with the larger freestream turbulence intensity. As the Reynolds number is increased in Figs. 9d, 9f and 10, with a freestream turbulence level of 8.1 %, the magnitude of the velocity deficit and the width of the wake continuously decrease. This trend correlates directly with the loss coefficient plotted in Fig. 4.

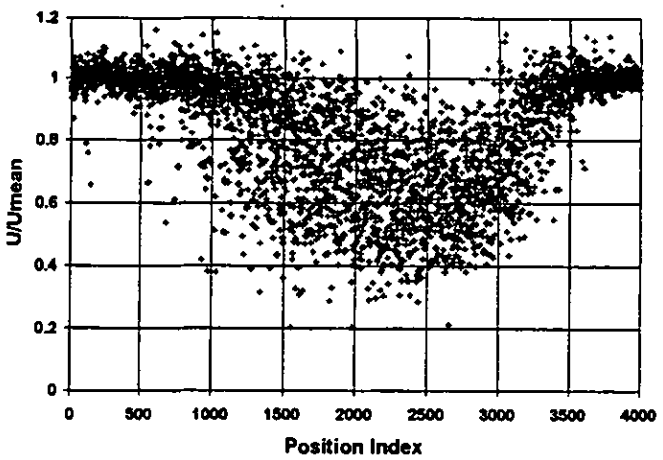

Figure 9a. Instantaneous Velocity Wake Survey, Re = 50k, Tu = 1.1%

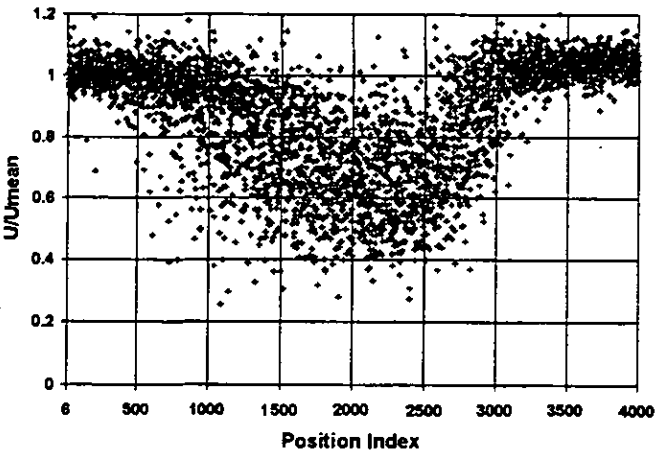

Figure 9b. Instantaneous Velocity Wake Survey, Re = 50k, Tu = 8.1%

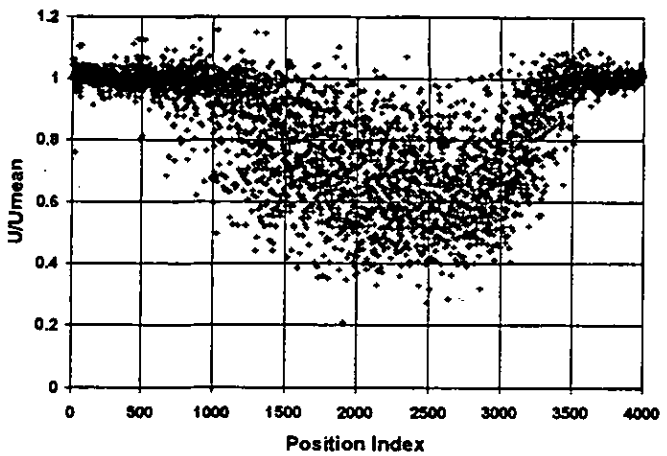

Figure 9c. Instantaneous Velocity Wake Survey, Re =100k, Tu = 1.1%

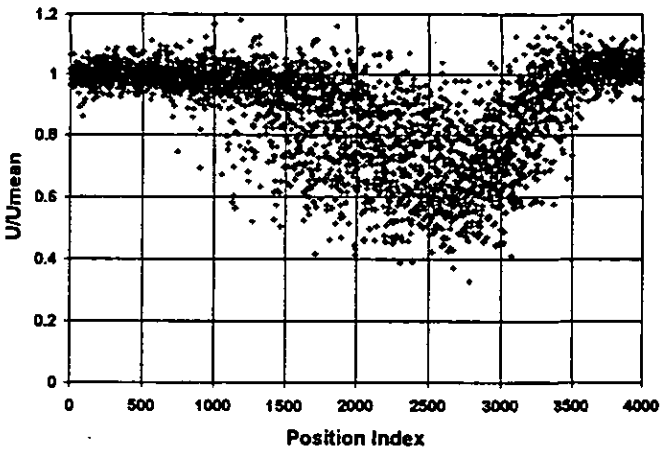

Figure 9d. Instantaneous Velocity Wake Survey, Re =100k, Tu = 8.1%

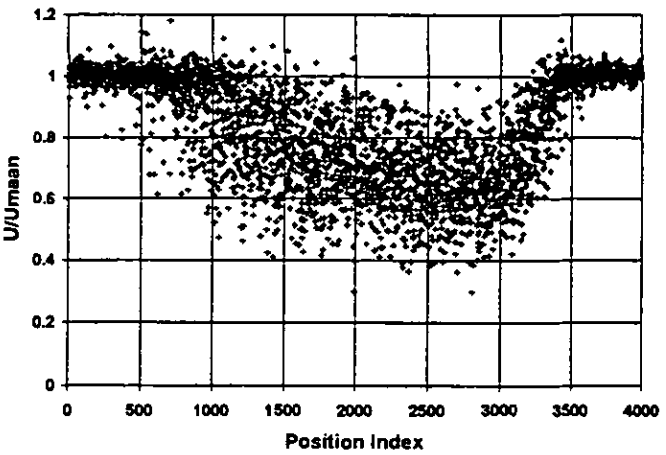

Figure 9e. Instantaneous Velocity Wake Survey, Re =200k, Tu = 1.1%

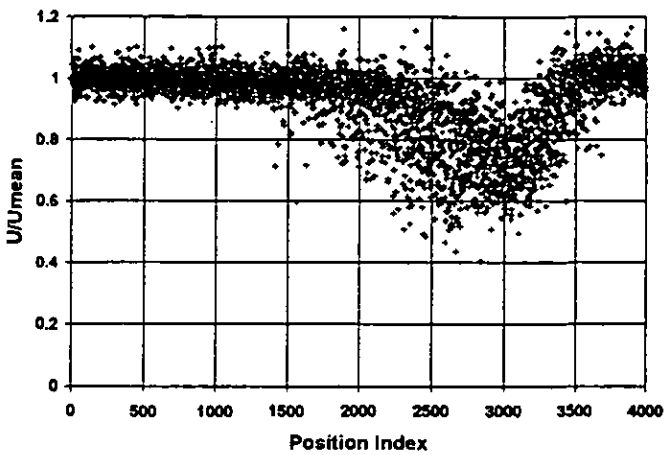

Figure 9f. Instantaneous Velocity Wake Survey, Re = 200k, Tu = 8.8%

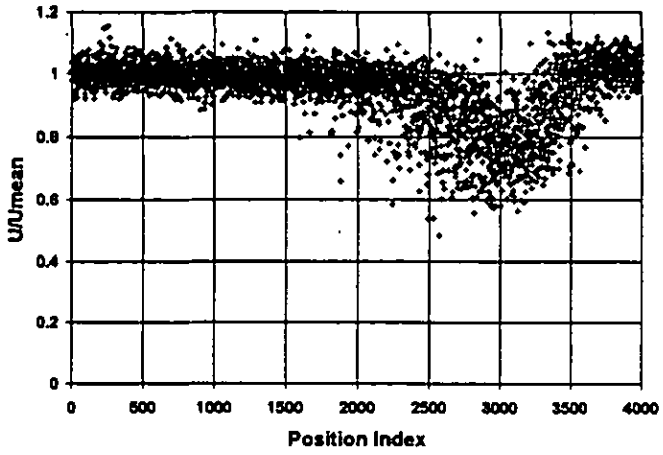

Figure 10. Instantaneous Velocity Wake Survey, Re = 300k, Tu = 8.8%

Figure 10 illustrates the local instantaneous velocity in the wake for Reynolds number of 300,000 and a freestream turbulence intensity of 8.1%. The wake is symmetric and the velocity defect is the smallest of the cases tested. The losses from the blade decrease as the Reynolds number and freestream turbulence are increased.

Figure 11 shows surveys of total pressure within wake which provides a measure of the local loss. The survey was conducted at the same streamwise location as the surveys in Fig. 9. In Fig. 11, the center of the trailing edge of the test blade is at 9.30 cm, the suction side of the wake would be at values greater than 9.30 cm, and the pressure side of the wake would be at values less than 9.30 cm. The local loss coefficient is defined by equation 1, substituting $P_{T_{exit}}$ for $\overline{P_{T_{exit}}}$.

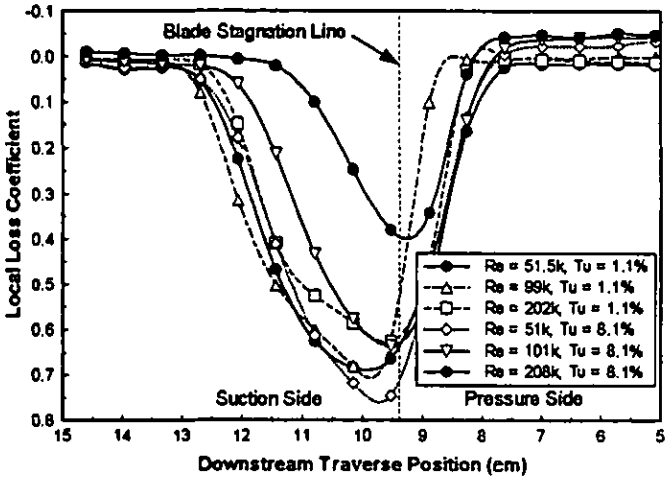

Figure 11. Local Loss Coefficient In The Wake

The same trends seen in Fig. 9 also apply to Fig. 11. The peak values of local loss coefficient move toward the pressure side as Reynolds number increases, for all values of freestream turbulence intensity. This trend was seen by Wunderwald and Fottner (1995) for a wake traverse in a compressor cascade. The peak in the local loss coefficient moves because the boundary layer thickness at the end of the turbine blade decreases as Reynolds number increases, as seen in Fig. 5. At higher Reynolds numbers, the flow is attached at the end of the suction surface. The survey in Fig. 11 is taken 2.54 cm behind the blade set. Some mixing of the detached boundary layers and the freestream occurs. At the lower Reynolds numbers, the thicker boundary layer, caused by flow separation at the rear of the suction surface, creates a larger local pressure drop, and more mixing occurs on the suction side of the wake.

CONCLUSION

The present study investigated the effects of Reynolds number and freestream turbulence intensity on a low pressure turbine cascade blade. Separation was observed at all Reynolds numbers and freestream turbulence intensities in this experimental study.

For a constant freestream turbulence of 1.1%, as the Reynolds numbers increase, the length and height of the separation zone decrease. Increasing Reynolds numbers also reduces velocity deficit in the wakes, but does not reduce the width of the wake. The loss coefficient decreases sharply as Reynolds number is increased to 100,000. Further increases in Reynolds numbers beyond 100,000 do not greatly affect the loss coefficient.

For cases with a freestream turbulence intensity of 8.1%, as Reynolds numbers increase, the suction side boundary layer, loss coefficient and pressure distributions change continuously. With increasing Reynolds number, the separation zone becomes smaller, reducing the velocity defect, and decreasing the wake width. This trend continues until the wake profile is almost symmetric with a Reynolds number of 300,000 and turbulence intensity of 8.1%.

At Reynolds numbers above 100,000, the higher turbulence intensity cases result in lower loss coefficients as a result of the smaller separation zones and reattachment of the boundary layer on the suction side.

ACKNOWLEDGEMENTS

The authors are grateful for the support from the AFOSR summer visiting scholar program. Also, we acknowledge the professional advice and assistance from members of the Wright Laboratory Basic Aerothermal Research team: namely Mr. David Pestian and Dr. Shichuan Ou. The authors are grateful for the support of Dr. Paul King of the AFIT Aeronautical Engineering Department for use of the linear cascade, and the AFIT model shop for rig modifications and upgrades.

REFERENCES

Baldwin, B. S., and Lomax, H., 1978, "Thin-Layer Approximation and Algebraic Model for Separated Turbulent Flows," AIAA Paper 78-0257.

Baughn, J.W., Butler, R.J., Byerley, A.R., and Rivir, R.B., 1995. An Experimental Investigation of Heat Transfer, Transition and Separation on Turbine Blades at Low Reynolds Number and High Turbulence Intensity. 1995 International Mechanical Engineering Congress and Exposition, San Francisco.

Gaster, M., 1966. The structure and Behavior of Laminar Separation Bubbles. AGARD-CP-4, pp. 819-854.

Halstead, D.E., Wisler, D.C., Okiishi, T.H., Walker, G.J., Hodson, H.P., and Shin, H-W., 1995. Boundary Layer Development in Axial Compressors and Turbines Part 4 of 4: Computations and Analysis. ASME paper No. 95-GT-464.

Kline, S.J. and McClintock, F.A., 1953. Describing Uncertainties in Single-Sample Experiments. Mechanical Engineering, Vol. 75, pp. 3-8.

Mayle, R.E., 1991. The Role of Laminar-Turbulent Transition in Gas Turbine Engines. ASME Paper No. 91-GT-282.

Rao, K. V., Delaney, R. A., and Dunn M. G., "Vane-Blade Interaction in a Transonic Turbine, Part 1 Aerodynamics," May-June 1994, Journal of Propulsion and Power, Vol. 10 No. 3, pp. 305-311.

Rivir, R., 1996. Transition on Turbine Blades and Cascades at Low Reynolds Numbers. AIAA Paper No. AIAA 96-2079.

Rivir, R., Sondergaard, R., Dahlstrom, M., and Ervin, E., 1996. Low Reynolds Number Turbine Blade Cascade Calculations. ISROMAC-6, The 6th International Symposium on Transport Phenomena and Dynamics of Rotating Machinery, Honolulu, HA,, Vol. II, pp 132-141.

Sharma, O.P., Ni, R.H., and Tanrikut, S., 1994. Unsteady Flows in Turbines - Impact on Design Procedure. AGARD-LS-195, Paper No. 5.

Wunderwald, D., and Fottner, L., 1995. Experimental Investigation of Boundary Layer Transition and Turbulence Structures on a Highly Loaded Compressor Cascade. ASME Paper No. 95-GT- 129.